Perovskite Quantum Dot LEDs

Deutsche Ausgabe: DOI: 10.1002/ange.201603698
Internationale Ausgabe: DOI: 10.1002/anie.201603698

Mesoporous Silica Particles Integrated with All-Inorganic $CsPbBr_3$ Perovskite Quantum-Dot Nanocomposites (MP-PQDs) with High Stability and Wide Color Gamut Used for Backlight Display

*Hung-Chia Wang, Shin-Ying Lin, An-Cih Tang, Bheeshma Pratap Singh, Hung-Chun Tong, Ching-Yi Chen, Yu-Chun Lee, Tzong-Liang Tsai, and Ru-Shi Liu**

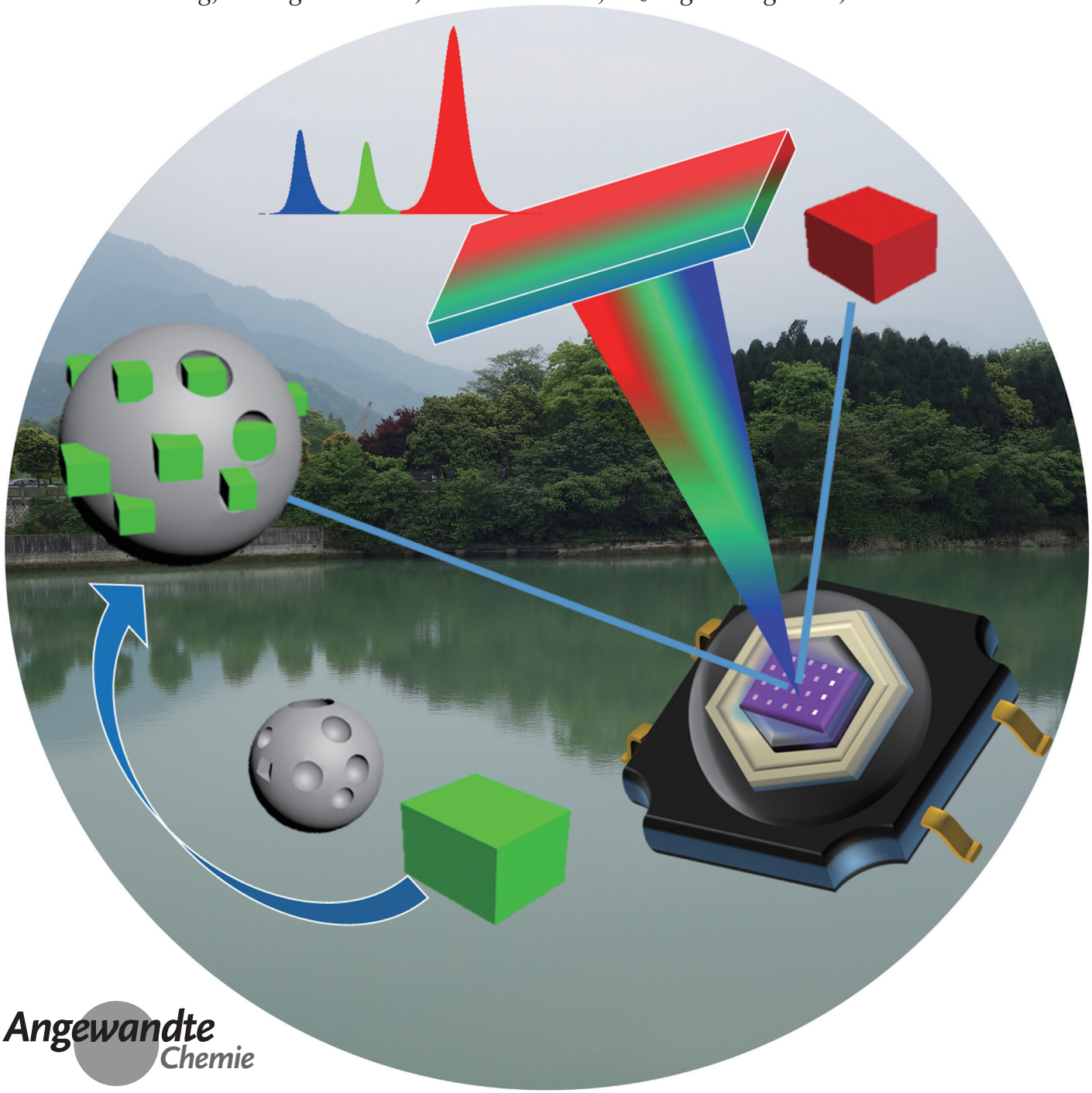

Abstract: *All-inorganic $CsPbX_3$ (X = I, Br, Cl) perovskite quantum dots (PQDs) have been investigated because of their optical properties, such as tunable wavelength, narrow band, and high quantum efficiency. These features have been used in light emitting diode (LED) devices. LED on-chip fabrication uses mixed green and red quantum dots with silicone gel. However, the ion-exchange effect widens the narrow emission spectrum. Quantum dots cannot be mixed because of anion exchange. We address this issue with a mesoporous PQD nanocomposite that can prevent ion exchange and increase stability. We mixed green quantum-dot-containing mesoporous silica nanocomposites with red PQDs, which can prevent the anion-exchange effect and increase thermal and photo stability. We applied the new PQD-based LEDs for backlight displays. We also used PQDs in an on-chip LED device. Our white LED device for backlight display passed through a color filter with an NTSC value of 113 % and Rec. 2020 of 85 %.*

Quantum dots (QDs) can be used in many applications, such as light emitting diodes (LEDs),[1] organic LEDs OLEDs,[2] solar cells,[3] and bioimaging.[4] QDs are an excellent candidate for backlight displays because of their high luminescence, narrow emission wavelength, and tunable color. QD-based white LEDs have been widely explored and have been further subdivided into two categories: one category is based on lighting[5] and the other category is used for backlight. These two categories are entirely different. For lighting, the most important factors are color rendering index (CRI) and luminescence at 1931 CIE coordinates (0.33, 0.33). The most general commercially available approach is the YAG phosphor mixed with silicone gel and InGaN blue placed on LED. However, its CRI is low. To increase CRI, we can mix red (R) phosphor with green (G) phosphor, but green phosphor exhibits low efficiency and entails high costs for this RG phosphor with a blue chip.[6] RG QDs have been commonly used in LED[5b] because their emission wavelengths can be simply tuned to increase luminescence and its CRI. QDs are optimum backlight materials because of their narrow emission wavelength and superior color purity. QD-based white LEDs exhibit advantage over conventional lightening owing to its design flexibility and optimization of the color performance and NTSC value through color filters.[7] The NTSC for commercial LCDs and wide-color-gamut TVs are approximately 72 % and 96 %, respectively. The NTSC for CdSe QD-based white LED devices reaches 104 % at CIE coordinates (0.24, 0.21).[1] During LED fabrication, packaging approaches should also be considered. On-film type[8] is the most common packaging approach; in this approach, QDs are in a thin-film form and placed over an entire display area. The demand on materials in this approach is much higher than that of other approaches. In this study, fabricated on-chip type QDs can decrease the demand on materials and provide a convenient packaging technique. Two types of perovskite-based semiconductors have been used: hybrid perovskite semiconductors and all-inorganic perovskite QDs. An example of a hybrid perovskite semiconductor is $MAPbX_3$ ($MA = CH_3NH_3$, X = Cl, Br, I) that can be potentially used for solar cells.[9] An organic ligand (MA) can be replaced with a cesium cation to develop a new type of perovskite semiconductor, namely, all-inorganic perovskite QDs.[10] For example, all-inorganic perovskite QD $CsPbX_3$ (X = Cl, Br, I) can be used more efficiently than Cd-based QD (CdSe)[11] and Cd-free QD (InP,[12] $CuInS_2$[13]) systems for backlight displays. Cd-based QDs for backlight display have also been extensively explored because of their high quantum efficiency and narrow emission wavelength. However, Cd-based (CdSe, CdTe) QDs have been synthesized under harsh reaction conditions and long reaction time; these conditions limit their commercial production. Cd-based QDs are also restricted in many countries because of the development of green chemistry. Cd-free InP QDs should be improved in terms of their quantum efficiency, and their full width to half-maximum should be decreased to enhance their color purity. In 2015, Protesescu et al.[10] reported a facile method to synthesize all-inorganic PQDs at a reaction temperature of approximately 180 °C and a reaction time of 5 s. Synthesizing PQDs with high quantum efficiency ($CsPbBr_3$ up to 90 %) and narrow emission wavelength (12–42 nm) is easier than fabricating traditional QDs. In all-inorganic PQDs with a tunable wavelength, their halide ratio and core growth temperature can be easily tuned to obtain different emission wavelengths. Furthermore, recently researchers used a fast anion-exchange method[14] to tune different emission wavelengths by adding Grignard reagents (MeMgX) or oleylammonium halides (OAmX) to $CsPbX_3$. Our research focuses on the synthesis and fabrication of PQDs and their use for backlight displays. The use of all-inorganic PQDs for LEDs is challenging. In a previous study, a silica coating on QDs was used to improve stability;[15] the most common methods are Stöber[16] and reverse microemulsion[17] methods. In silica coating, surface ligand exchange initially occurs and phase changes from oil to water. Ligand exchange is difficult to facilitate because of the low stability of PQDs. Other polymer encapsulating methods also encounter issues on solvent polarity.[18] Generally the strong anion-exchange effect was observed when green and red all-inorganic QDs were mixed with silicone resin.

We propose an efficient and simple method to prevent the anion-exchange effect. We mixed green $CsPbBr_3$ PQDs with purchased mesoporous silica[19] whose pore size is approximately 12–15 nm. The synthesis is shown in Scheme 1. We can use non-polar solvents, such as hexane and toluene, to prevent the solvent effect of polymers and to synthesize mesoporous silica green PQD nanocomposite (MP-G-PQDs; Scheme 1) with mesoporous silica.

[*] H. C. Wang, S. Y. Lin, A. C. Tang, Dr. B. P. Singh, Prof. Dr. R. S. Liu
Department of Chemistry
National Taiwan University
Taipei, 106 (Taiwan)
E-mail: rsliu@ntu.edu.tw
Prof. Dr. R. S. Liu
Department of Mechanical Engineering and Graduate Institute of Manufacturing Technology, National Taipei University of Technology
Taipei 106 (Taiwan)
H. C. Tong, Dr. C. Y. Chen, Dr. Y. C. Lee, Dr. T. L. Tsai
Lextar Electronic Corporation
Hsinchu, 300 (Taiwan)

Supporting information for this article can be found under: http://dx.doi.org/10.1002/anie.201603698.

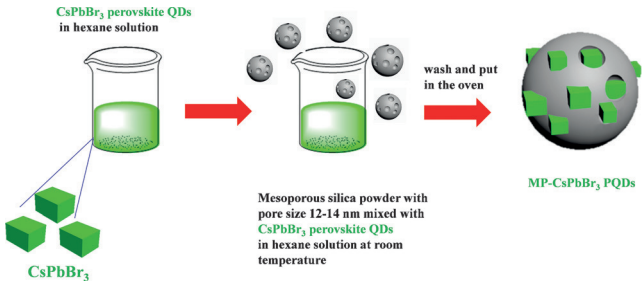

Scheme 1. The synthesis process of mesoporous silica green PQD nanocomposite (MP-PQDs).

All-inorganic $CsPbX_3$ (X = Cl, Br, I) QDs were synthesized by using previous methods. We tuned different Br/I and Br/Cl ratios to obtain various emission wavelengths. In the application of white LED (photoluminescence) and QD-LED (electroluminescence), red–green–blue (RGB) PQDs are the most important applications. Figure 1 shows the emission and UV/Vis spectra of RGB PQDs. We synthesized

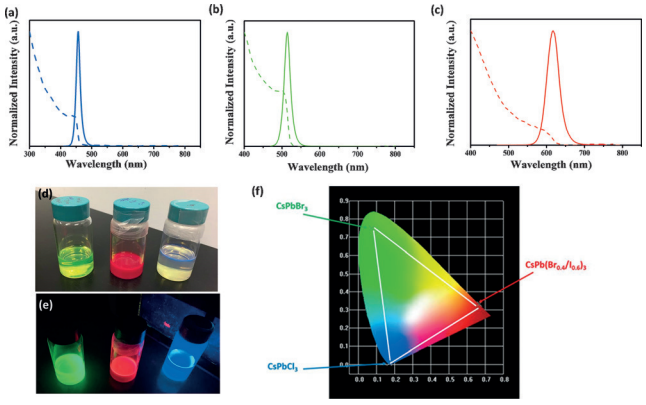

Figure 1. Photoluminescence and UV/Vis spectra of a) blue $CsPb(Br_{0.5}Cl_{0.5})_3$, b) green $CsPbBr_3$, and c) red $CsPb(Br_{0.4}I_{0.6})_3$ perovskite QDs. Colloidal RGB PQDs dispersed in d) hexane under sunlight, e) hexane under UV-light (365 nm) and f) color gamut spectra of RGB PQDs.

blue (460 nm) $CsPb(Br_{0.5}Cl_{0.5})_3$, green (515 nm) $CsPbBr_3$, and red (625 nm) $CsPb(Br_{0.4}I_{0.6})_3$ QDs with a narrow emission bandwidth of 15 nm (blue), 20 nm (green), and 30 nm (red). For backlight applications, the CIE coordinates of blue (0.17, 0.01), green (0.07, 0.75), and red (0.66, 0.34) are shown in Figure 1 f. The wide color gamut spectra of RGB PQDs are attributed to the narrow emission wavelength.

The PL and UV/Vis spectra of different ratios of $CsPb(Br_{1-x}I_x)_3$ are shown in Figure S1 in the Supporting Information. The emission spectra can be tuned from 515 nm to 690 nm by adjusting the different halide ratios. UV/Vis spectra revealed the first absorption maximum peak shifted because of different halide ion ratios. The quantum yield of $CsPbX_3$ PQDs was measured by using an absolute photoluminescence quantum yield spectrometer (c11347, HAMAMATSU). An excitation wavelength of 460 nm was set to calculate the quantum yield in an InGaN blue chip. Figure S2a illustrates the absolute quantum yield and full-width at half wavelength of $CsPbX_3$ PQDs with different emission wavelengths (457–698 nm). The absolute quantum yields of green $CsPbBr_3$ and red $CsPb(I_{0.6}Br_{0.4})_3$ were 55% and 70%, respectively. The full width of half wavelength of $CsPbX_3$ PQDs were approximately 13–35 nm.

As shown in Figure 2, the red shift of emission wavelength decreases with the increasing average particle size of the RGB PQDs. This phenomenon indicated that the emission wavelength of PQDs was dominated by the halide ratio and quantum size effect. $CsPbX_3$ was cubic, which is a highly stable structure.

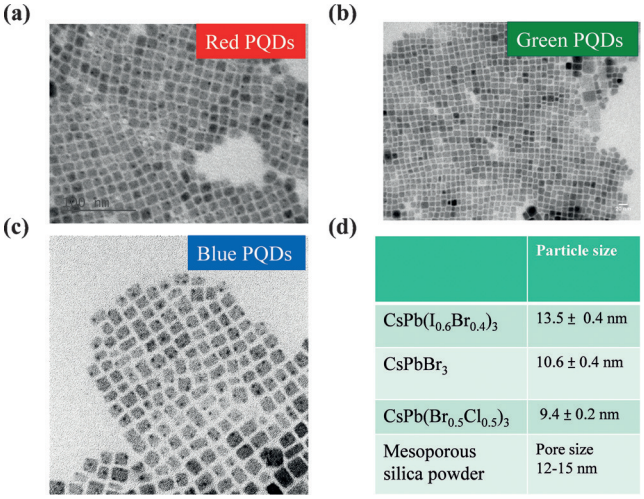

	Particle size
$CsPb(I_{0.6}Br_{0.4})_3$	13.5 ± 0.4 nm
$CsPbBr_3$	10.6 ± 0.4 nm
$CsPb(Br_{0.5}Cl_{0.5})_3$	9.4 ± 0.2 nm
Mesoporous silica powder	Pore size 12-15 nm

Figure 2. TEM spectra of a) blue $CsPb(Br_{0.5}Cl_{0.5})_3$, b) green $CsPbBr_3$, c) red $CsPb(Br_{0.4}I_{0.6})_3$ perovskite QDs, and d) Particle size of RGB perovskite QDs and pore size of mesoporous silica powder.

$CsPbX_3$ PQDs crystallize to form an orthorhombic or cubic phase because of the synthesis temperature. In our synthesis, the reaction temperature was approximately 170–190 °C; therefore, the phase of our $CsPbX_3$ QDs is cubic. Figure 3 a reveals $CsPbX_3$ with various Br/I ratios; the phase of $CsPbX_3$ was cubic in contrast to the standard phase of

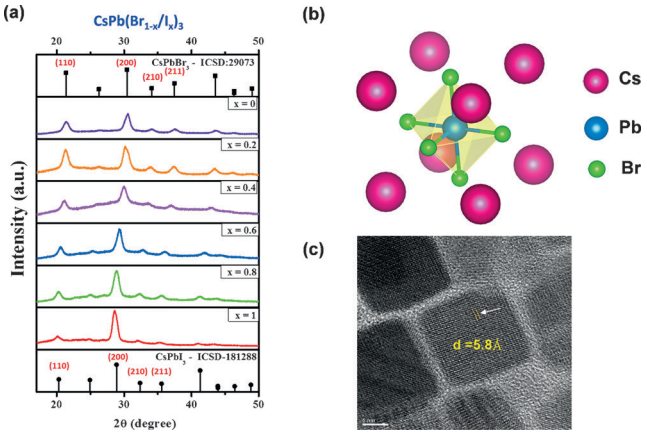

Figure 3. a) X-ray diffraction patterns of PQDs with various Br/I ratios, b) crystal structure of cubic $CsPbBr_3$, and c) high-resolution TEM images of $CsPbBr_3$ PQDs.

$CsPbI_3$ (ICSD-181288), $CsPbBr_3$ (ICSD-29073), and $CsPbCl_3$ (ICSD-29072). The XRD result with various Br/Cl ratios is shown in Figure S3.

For structural characterization, high-resolution-TEM results are shown in Figure 3c. Green $CsPbBr_3$ PQDs were single-crystalline cubic phase with *d*-spacing of 5.8 Å. Elemental analysis was performed by using an energy dispersive X-ray analyzer (EDS) to confirm the elemental composition ratios of green $CsPbBr_3$ QDs (Figure S4). The element ratio of Cs, Pb, and Br was approximately 1:1:3, which fitted the experimental ratio.

$CsPbBr_3$ QDs with 10 nm particle size and cubic phase structure were integrated with mesoporous silica nanoparticles. A RGB MP-PQD nanocomposite is illustrated in Figure 4. The mesoporous silica material was purchased.

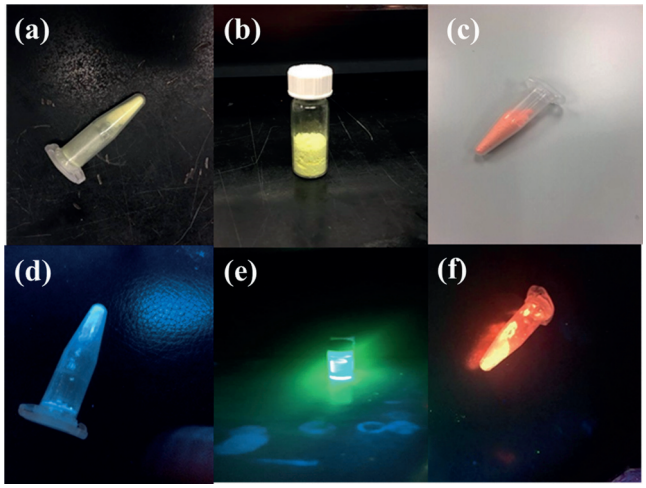

Figure 4. a) Blue, b) green, and c) red MP-PQDs under sunlight illumination. d) Blue, e) green, and f) red MP-PQDs under UV light (365 nm) excitation.

The TEM and SEM images of mesoporous silica nanoparticles are shown in Figure S5. The size of this mesoporous silica nanoparticle was 200–500 nm and its pore size was approximately 12–15 nm. The PL spectrum of MP-$CsPbBr_3$ and $CsPbBr_3$ is shown in Figure S6. The emission wavelength of MP-$CsPbBr_3$ was shifted approximately 4 nm from 515 nm to 519 nm. The stability of PQDs can be enhanced by this novel PQD nanocomposite. If we aim to use PQDs in an on-chip system, we should improve the stability of PQDs.

We used a thermal controller system to test the thermal stability (Figure 5). The experimental temperature ranged from 25 °C to 100 °C. The relative intensity of $CsPbBr_3$ PQDs decreased when the temperature increased. The thermal cycling results were shown in Figure S7. MP-$CsPbBr_3$ exhibited higher thermal stability and thermal recycling than $CsPbBr_3$. When the temperature was decreased to room temperature, the intensity of MP-$CsPbBr_3$ was nearly the same as that before the temperature treatment. The relative intensity of green $CsPbBr_3$ PQDs was decreased to 60 % after heat treatment was administered.

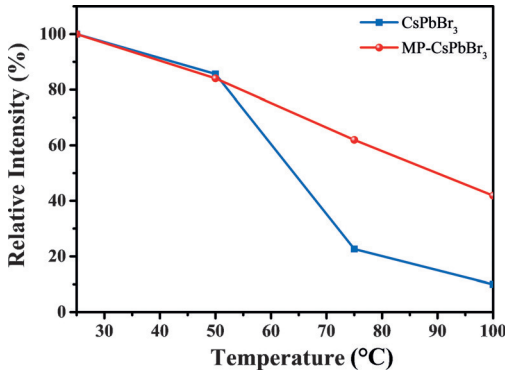

Figure 5. Thermal stability test of MP-$CsPbBr_3$ and $CsPbBr_3$.

A photostability test of $CsPbBr_3$ PQDs was implemented under continuous UV-light (365 nm, 6 W) irradiation. The test period was from 30 min to 96 h. In Figure 6, $CsPbBr_3$ PQDs were dispersed in hexane and exposed to UV light irradiation for 96 h. After 96 h, the relative intensity of $CsPbBr_3$ was decreased to 40 %. As seen for previously designed core/shell structures of QDs, a passivation shell[20] can prevent photooxidation during UV light irradiation.

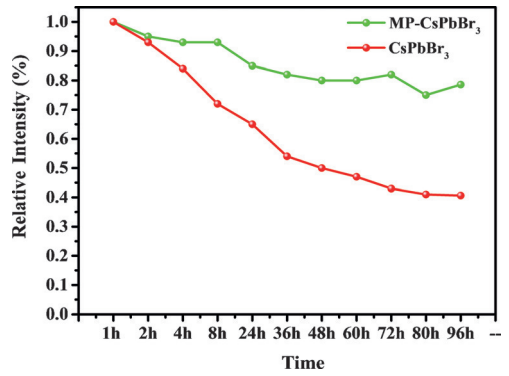

Figure 6. Photostability test of MP-$CsPbBr_3$ and $CsPbBr_3$.

However, PQDs only have a core structure, which is easily exposed to oxygen and thus causes surface defects. The relative intensity decreased quickly and because of surface defects, and PQDs decomposed. We also observed some $CsPbBr_3$ residues after the PQDs were exposed to UV light irradiation. The mesoporous silica shell can act as a protective shell for the core of $CsPbBr_3$ PQDs. After 96 h, MP-$CsPbBr_3$ powder is approximately equal to 80 % under UV light irradiation. MP-$CsPbBr_3$ nanocomposite not only exhibits better thermal and photostability but also resolves the anion-exchange phenomena of PQDs.

In LED packaging, green $CsPbBr_3$ was initially mixed with red $CsPb(Br_{0.4}I_{0.6})_3$ PQDs in silicone resin and then dropped in the blue chip. The spectra of green $CsPbBr_3$ PQDs and red $CsPb(Br_{0.4}I_{0.6})_3$ PQDs under the excitation of the blue chip (450 nm) are shown in Figure 7. The emission wavelengths of green and red QDs were 515 and 625 nm, respectively. The mixture spectra are also illustrated in

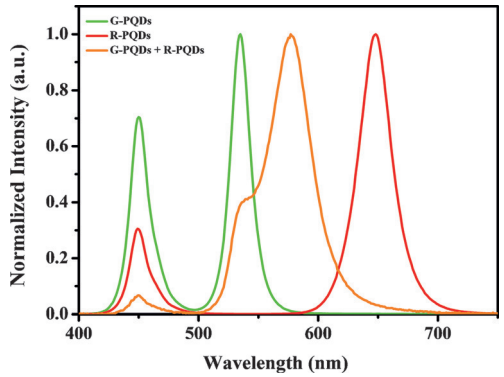

Figure 7. Spectra of green, red, and mixed (green + red) PQDs was under the excitation of a 450 nm blue chip.

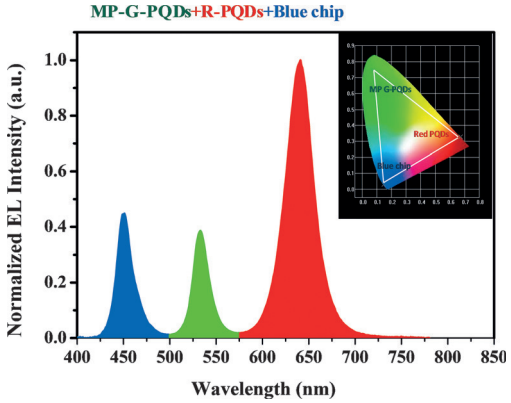

Figure 8. Spectra of MP-$CsPbBr_3$ mixed with red PQDs under blue chip (450 nm) excitation. The inset spectrum reveals the color gamut of white light LED.

Figure 7. Red and green strongly shifted to yellow when the narrow emission spectra widened. Considering the strong ion-exchange effect, we cannot use this narrow emission wavelength and high quantum yield of PQDs for LEDs.

Green MP-PQD nanocomposite was mixed with red perovskite QDs in silicone resin to solve this problem. The obtained spectra are shown in Figure 8. No spectrum shift of this device was observed. The color coordinates of red PQDs and MP-green PQDs were (0.66, 0.34) and (0.19, 0.69), respectively.

A wide color gamut was also determined as shown in Figure 9. The color coordinates of the PQD-white LED were optimized at (0.24, 0.28) in CIE 1931 and luminous efficiency 30 lm/w. We first successfully used PQDs packaged on-chip in a backlight display. The advantages of PQDs included a narrower emission wavelength and a higher quantum efficiency than those of traditional QDs. For backlight display, the NTSC value of the device should also be calculated. The emission wavelengths of RGB before the PQDs were filtered were 625, 519, and 450 nm. PQD-white LED passed through the color filter The RGB CIE coordinates were (0.69, 0.30), (0.19, 0.73), and (0.14, 0.04) after the PQDs were passed through the color filter. The color gamut overlap of the NTSC space was approximately 113%, which was higher than a previously designed regular phosphor LED (NTSC 86%) and Cd-QD LED (NTSC 104%). This result is attributed to the narrow emission wavelength of the green and red PQDs. The new definition of color space is Rec 2020. The RGB CIE coordinates were (0.70, 0.29), (0.17, 0.79), and (0.13, 0.04) because of the wider color gamut of the display. The overlap area of the Rec 2020 of the PQD-white LED was approximately 85%.

In summary, the anion-exchange phenomenon of all-inorganic PQDs was successfully resolved. In previous studies, the anion-exchange effect is a simple mechanism used to tune wavelengths. In LED packaging, this effect should be prevented. We created a mesoporous PQD nanocomposite, which can prevent the anion exchange and increase stability. We mixed green MP-$CsPbBr_3$ PQD nanocomposite with red PQDs in silicon resin and subjected to excitation by using a blue InGaN chip. Our white LED device for backlight display was passed through a color filter. The NTSC value is 113% and the Rec 2020 value is 85%.

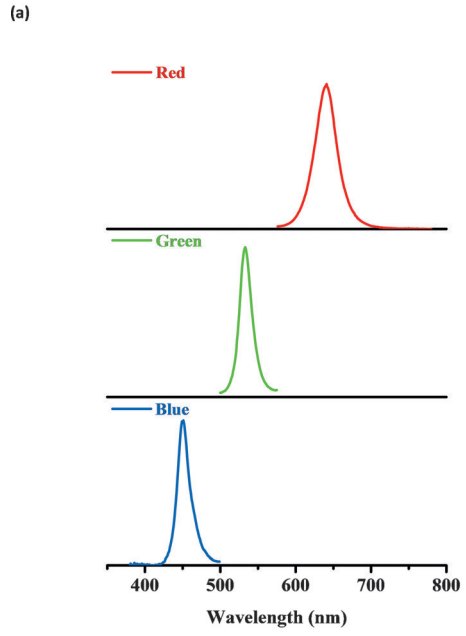

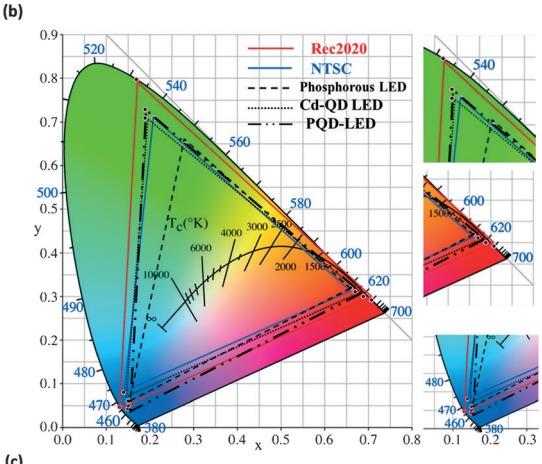

(c)

Name	NTSC	(x,y)	Reference
Phosphorous LED	86	=	[1]
Cd-QD LED	104	(0.24,0.21)	[1]
PQD-LED	113	(0.24,0.28)	=

Figure 9. a) Spectra of PQD-based white LED before color filter, b) color gamut of PQD-LED, phosphor LED, and Cd-QDs white LED c) The table features data of the three types of display.

Experimental Section

Typical synthesis process of colloidal $CsPbBr_3$ perovskite QDs followed the previous procedure. The detailed synthesis process was shown in Supporting Information. Synthesized mesoporous silica $CsPbBr_3$ perovskite QDs nanocomposite (MP-PQDs): 10 mg mL^{-1} green $CsPbBr_3$ was mixed with 100 mg mesoporous silica powder in hexane solution and stirred for 1 h. After that, the precipitate was collected by centrifugation at 4000 rpm and solvent was removed for 30 min at 40 °C. We can obtain MP-PQDs nanocomposite powder.

Acknowledgements

We thank the Ministry of Science and Technology of Taiwan (Contract No. MOST 104-2113-M-002-012-MY3) for financially supporting this research. This work is also supported by the Lextar Electronics Corporation. We also express our gratitude to Ms. C. Y. Chien of the Precious Instrument Center (National Taiwan University) for her assistance in our TEM experiments.

Keywords: all-inorganic perovskite quantum dots · backlight · light emitting diode · white light

How to cite: *Angew. Chem. Int. Ed.* **2016**, *55*, 7924–7929
Angew. Chem. **2016**, *128*, 8056–8061

[1] E. Jang, S. Jun, H. Jang, J. Lim, B. Kim, Y. Kim, *Adv. Mater.* **2010**, *22*, 3076–3080.
[2] a) K. H. Lee, C. Y. Han, H. D. Kang, H. Ko, C. Lee, J. Lee, N. Myoung, S. Y. Yim, H. Yang, *ACS Nano* **2015**, *9*, 10941–10949; b) J. R. Manders, L. Qian, A. Titov, J. Hyvonen, J. T. Scott, K. P. Acharya, Y. Yang, W. Cao, Y. Zheng, J. Xue, P. H. Holloway, *J. Soc. Inf. Disp.* **2015**, *23*, 523–528.
[3] I. Robel, V. Subramanian, M. Kuno, P. V. Kamat, *J. Am. Chem. Soc.* **2006**, *128*, 2385–2393.
[4] a) K. T. Yong, I. Roy, R. Hu, H. Ding, H. Cai, J. Zhu, X. Zhang, E. J. Bergey, P. N. Prasad, *Integr. Biol.* **2010**, *2*, 121–129; b) C. W. Chen, D. Y. Wu, Y. C. Chan, C. C. Lin, P. H. Chung, M. Hsiao, R. S. Liu, *J. Phys. Chem. C* **2015**, *119*, 2852–2860.
[5] a) A. Aboulaich, M. Michalska, R. Schneider, A. Potdevin, J. Deschamps, R. Deloncle, G. Chadeyron, R. Mahiou, *ACS Appl. Mater. Interfaces* **2014**, *6*, 252–258; b) S. H. Park, A. Hong, J. H. Kim, H. Yang, K. Lee, H. S. Jang, *ACS Appl. Mater. Interfaces* **2015**, *7*, 6764–6771.
[6] S. Neeraj, N. Kijima, A. K. Cheetham, *Chem. Phys. Lett.* **2004**, *387*, 2–6.
[7] W. G. Bi, F. Zhao, X. F. Jiang, *Optoelectronics Global Conference (OGC)* **2015**, 1–3.
[8] S. Coe-Sullivan, W. Liu, P. Allen, J. S. Steckel, *ECS J. Solid State Sci. Technol.* **2013**, *2*, 3026–3030.
[9] W. Zhang, M. Anaya, G. Lozano, M. E. Calvo, M. B. Johnston, H. Míguez, H. J. Snaith, *Nano Lett.* **2015**, *15*, 1698–1702.
[10] L. Protesescu, S. Yakunin, M. I. Bodnarchuk, F. Krieg, R. Caputo, C. H. Hendon, R. X. Yang, A. Walsh, M. V. Kovalenko, *Nano Lett.* **2015**, *15*, 3692–3696.
[11] A. Swarnkar, R. Chulliyil, V. K. Ravi, M. Irfanullah, A. Chowdhury, A. Nag, *Angew. Chem. Int. Ed.* **2015**, *54*, 15424–15428; *Angew. Chem.* **2015**, *127*, 15644–15648.
[12] S. J. Yang, J. H. Oh, S. Kim, H. Yang, Y. R. Do, *J. Mater. Chem. C* **2015**, *3*, 3582–3591.
[13] P. H. Chuang, C. C. Lin, R. S. Liu, *ACS Appl. Mater. Interfaces* **2014**, *6*, 15379–15387.
[14] a) G. Nedelcu, L. Protesescu, S. Yakunin, M. I. Bodnarchuk, M. J. Grotevent, M. V. Kovalenko, *Nano Lett.* **2015**, *15*, 5635–5640; b) P. Ramasamy, D. H. Lim, B. Kim, S. H. Lee, M. S. Lee, J. S. Lee, *Chem. Commun.* **2016**, *52*, 2067–2070; c) Q. A. Akkerman, V. D'Innocenzo, S. Accornero, A. Scarpellini, A. Petrozza, M. Prato, L. Manna, *J. Am. Chem. Soc.* **2015**, *137*, 10276–10281.
[15] a) D. K. Yi, S. T. Selvan, S. S. Lee, G. C. Papaefthymiou, D. Kundaliya, J. Y. Ying, *J. Am. Chem. Soc.* **2005**, *127*, 4990–4991; b) R. Kumar, H. Ding, R. Hu, K. T. Yong, I. Roy, E. J. Bergey, P. N. Prasad, *Chem. Mater.* **2010**, *22*, 2261–2267.
[16] W. Stöber, A. Fink, E. Bohn, *J. Colloid Interface Sci.* **1968**, *26*, 62–69.
[17] J. Ziegler, S. Xu, E. Kucur, F. Meister, M. Batentschuk, F. Gindele, T. Nann, *Adv. Mater.* **2008**, *20*, 4068–4073.
[18] Y. Kim, E. Yassitepe, O. Voznyy, R. Comin, G. Walters, X. Gong, P. Kanjanaboos, A. F. Nogueira, E. H. Sargent, *ACS Appl. Mater. Interfaces* **2015**, *7*, 25007–25013.
[19] W. Chen, K. Wang, J. Hao, D. Wu, S. Wang, J. Qin, C. Li, W. Cao, *Part. Part. Syst. Charact.* **2015**, *32*, 922–927.
[20] J. H. Jo, J. H. Kim, S. H. Lee, H. S. Jang, D. S. Jang, J. C. Lee, K. U. Park, Y. Choi, C. Ha, H. Yang, *J. Alloys Compd.* **2015**, *647*, 6–13.

Received: April 16, 2016
Published online: May 30, 2016

